Journal of Alloys and Compounds 579 (2013) 82–85

Contents lists available at SciVerse ScienceDirect

Journal of Alloys and Compounds

journal homepage: www.elsevier.com/locate/jalcom

Letter

Afterglow luminescence properties and mechanism of novel orange afterglow phosphor: $Ca_2Sb_2O_7:Sm^{3+}$

Liurong Shi, Jiachi Zhang *, Huihui Li *, Pengfei Feng, Xue Liu, Zhongqiu Fu, Yuhua Wang

Key Laboratory for Magnetism Magnetic Materials of the Ministry of Education, Lanzhou University, Lanzhou 730000, PR China

ARTICLE INFO

Article history:
Received 8 January 2013
Received in revised form 3 May 2013
Accepted 3 May 2013
Available online 17 May 2013

Keywords:
$Ca_2Sb_2O_7:Sm^{3+}$
Afterglow luminescence
Phosphor

ABSTRACT

A novel afterglow phosphor $Ca_2Sb_2O_7:Sm^{3+}$ with a weberite-type structure is synthesized using a solid state reaction at 1150 °C. The intense orange afterglow luminescence is first observed in antimonates ($Ca_2Sb_2O_7:Sm^{3+}$) and lasts for approximately 770 s (0.32 mcd/m^2). The afterglow emissions are composed of host emission and characteristic emission lines of Sm^{3+}. Further, the Sm^{3+} ions not only act as afterglow emission centers but also serve as aliovalent auxiliaries to create hole traps. The thermoluminescence indicates that at least two types of traps are created by doping Sm^{3+} ions, which are basically responsible for the afterglow luminescence of $Ca_2Sb_2O_7:Sm^{3+}$. Accordingly, the possible afterglow luminescence mechanism of $Ca_2Sb_2O_7:Sm^{3+}$ is proposed.

1. Introduction

Afterglow materials have attracted considerable attention for decades because of their widespread use in areas such as safety indication and emergency lighting [1–4]. The existing commercial afterglow tricolor phosphors are $SrAl_2O_4:Eu^{2+},Dy^{3+}$ (green), $CaAl_2O_4:Eu^{2+},Nd^{3+}$ (blue), and $Y_2O_2S:Eu^{3+},Ti^{3+},Mg^{2+}$ (red) [5–9]. However, there are still some deficiencies in the existing afterglow phosphors, and the afterglow luminescence mechanisms of afterglow phosphors are not yet clear. Therefore, it is necessary to explore the possibilities of other new systems that can be used as afterglow phosphors. Thus far, many novel inorganic materials doped with various activators have been developed as afterglow phosphors [1–3,10–12].

In general, the antimonates constitute a large family of wide-band-gap p-block semiconductors, diverse in structures and compositions [13–15]. Nevertheless, only a rather small number of Sb-containing compounds have been investigated as luminescence materials. To the best of our knowledge, the afterglow luminescence in antimonate systems has never been reported thus far. On the other hand, Sm^{3+} ion is generally considered as an excellent candidates as red emission centers and many novel Sm^{3+} ion doped phosphors have been widely reported [16–19].

In this study, the orthorhombic weberite $Ca_2Sb_2O_7:Sm^{3+}$ was synthesized by a solid state reaction at 1150 °C, and the most important observation was that of the intense orange afterglow luminescence in antimonates. The photoluminescence and the afterglow luminescence properties of the $Ca_2Sb_2O_7:Sm^{3+}$ samples were investigated in detail. According to the results, we have proposed a possible mechanism of the afterglow luminescence of $Ca_2Sb_2O_7:Sm^{3+}$ materials.

2. Experimental methods and details

A series of $Ca_2Sb_2O_7:Sm^{3+}$ samples were synthesized by a traditional solid state reaction: the raw materials were $CaCO_3$ (AR), Sb_2O_3 (AR), and Sm_2O_3 (99.99%). The ingredients were mixed thoroughly and then fired in alumina crucibles at 1150 °C for 16 h in air. Finally, the samples were cooled to room temperature slowly in the furnace and ground again with an agate mortar.

A Rigaku D/Max-2400 X-ray diffractometer (XRD) was employed to check the phase of the samples. The absorption spectra were obtained from diffuse reflection measurements using a UV–visible spectrophotometer (PE Lambda 950), and $BaSO_4$ was used as a reference. The excitation and emission spectra were measured with an FLS-920T fluorescence spectrophotometer fitted with a Xe900 lamp (450 W). The scan speed for the photoluminescence emission spectra was 30 nm/min, and the dwell time was 0.2 s. The scan speed for the afterglow emission spectra was 20 s per spectrum. The ex-slits for the photoluminescence (PL) excitation and emission spectra were 1 nm, and the em-slits for the afterglow spectra (AG) were 10 nm. The decay curve was then measured with a PR305 afterglow phosphorescence instrument at 15 °C. The thermoluminescence (TL) curve was measured using a FJ-427A TL meter (Beijing Nuclear Instrument Factory). The samples' weight was kept constant (3 mg). Prior to the measurements, powdery samples were heated from 273 to 673 K at the rate of 1 K/s. All of the other measurements were performed at room temperature.

3. Results and discussion

The XRD patterns for the representative samples are shown to verify the phase purity in Fig. 1. It is clear that all the observed peaks of the un-doped $Ca_2Sb_2O_7$ (a) and $Ca_2Sb_2O_7:0.008Sm^{3+}$ (b) samples can be indexed well with JCPDF#26-0293 (c), indicating

---

* Corresponding authors. Tel.: +86 931 8912772; fax: +86 931 891355.
E-mail addresses: zhangjch@lzu.edu.cn (J. Zhang), lihh@lzu.edu.cn (H. Li).

0925-8388/$ - see front matter © 2013 Elsevier B.V. All rights reserved.
http://dx.doi.org/10.1016/j.jallcom.2013.05.056

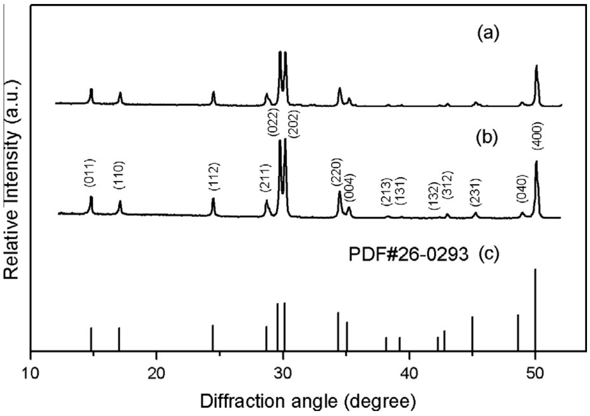

Fig. 1. Typical X-ray diffraction patterns for the samples: (a) is the XRD pattern for the $Ca_2Sb_2O_7$ material, (b) is the XRD pattern for $Ca_2Sb_2O_7$:$0.008Sm^{3+}$, and (c) is the pattern from JCPDS Standard Card No 26–0293 for the $Ca_2Sb_2O_7$ material.

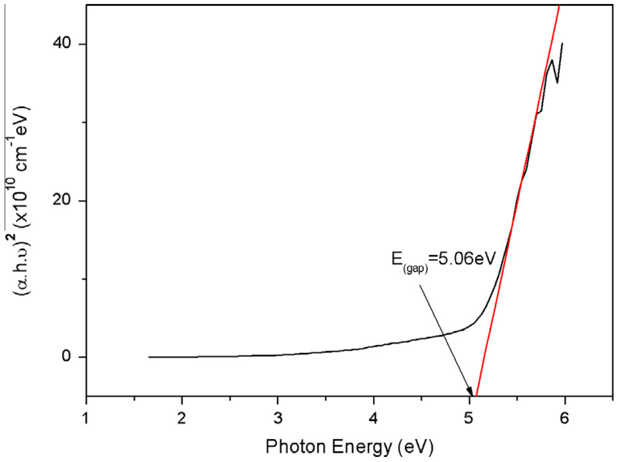

Fig. 3. Relationship of $(h\nu\alpha)^2$ and $h\nu$ of the $Ca_2Sb_2O_7$ sample.

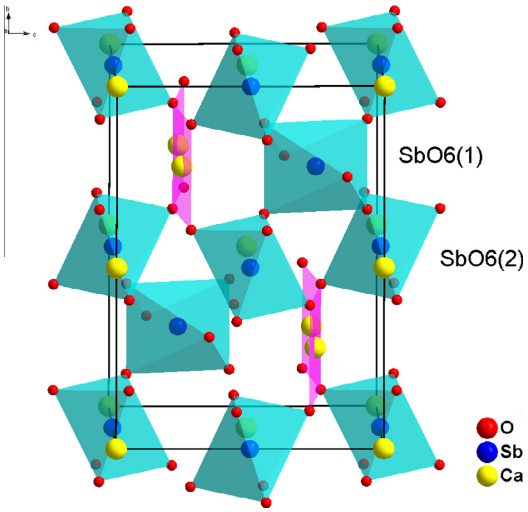

Fig. 2. Crystal structure and spheres for Sb^{5+} ions in the $Ca_2Sb_2O_7$ crystal.

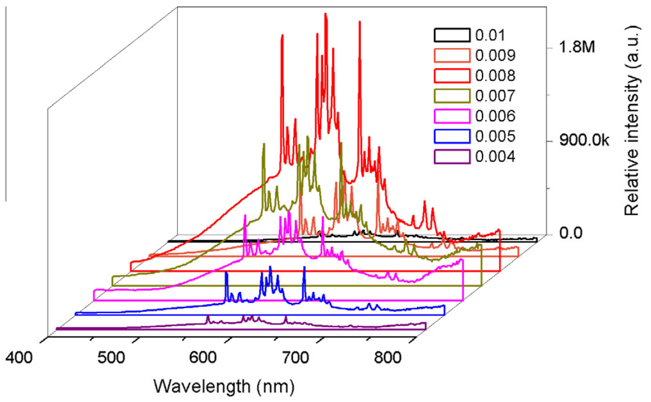

Fig. 4. Emission spectra of $Ca_2Sb_2O_7$ doped with different Sm^{3+} concentrations (Sm^{3+} concentration = 0.004, 0.005, 0.006, 0.007, 0.008, 0.009, 0.01) as representatives.

that the present samples were single phases. It can be deduced that the $Ca_2Sb_2O_7$ sample has an orthorhombic weberite structure with space group Imma (74) (a = 7.28 Å, b = 7.37 Å, c = 10.18 Å). Further, the doping of the Sm^{3+} ions does not induce impurity in the $Ca_2Sb_2O_7$ crystal. The coordination spheres for the Sb^{5+} ions in the orthorhombic weberite structure were drawn using the "Diamond 3" program and are shown in Fig. 2. It is observed that the $Ca_2Sb_2O_7$ crystal is composed of two types of SbO_6 groups. In particular, SbO_6 (1) exhibits a compressed octahedron structure, while SbO_6 (2) exhibits an elongated octahedral structure. The deformed SbO_6 octahedral may have some influence on its luminescence behavior. Rows of Ca^{2+} ions lie between the octahedron.

Fig. 3 illustrates the relationship of $(h\nu\alpha)^2$ and $h\nu$ of the $Ca_2Sb_2O_7$ sample. The absorption data were obtained from diffuse reflection measurements. The band gap energy is related to the absorbance and photon energy as shown in the following equation:

$$h\nu\alpha \propto (h\nu - E_g^{opt})^2 \qquad (1)$$

where α is the absorbance, h is the Planck constant, ν is the frequency, and E_g^{opt} is the optical band gap [20,21]. In this case, the optical band gap was determined by extrapolating the linear portion of the curve or tail. The result obtained for $Ca_2Sb_2O_7$ is 5.06 eV, indicating that the energy gap is sufficiently broad for $Ca_2Sb_2O_7$ to be a potential host for afterglow luminescence.

Fig. 4 shows the emission spectra (λ_{ex} = 254 nm) of $Ca_2Sb_2O_7$ doped with different Sm^{3+} concentrations (Sm^{3+} concentration = 0.004, 0.005, 0.006, 0.007, 0.008, 0.009, 0.01) as representatives. A broad emission band centered at 605 nm and some emission lines can be clearly observed. The broad emission band may be related to the deformation of the SbO_6 octahedral in the host lattice. These emission peaks in 550–700 nm correspond to the characteristic emissions of the Sm^{3+} ions and can be attributed to the splitting $^4G_{5/2} \rightarrow {}^6H_{5/2}$ (564, 569, 578, 585 nm), $^4G_{5/2} \rightarrow {}^6H_{7/2}$ (595, 602, 607, 611, 619, 624 nm), and $^4G_{5/2} \rightarrow {}^6H_{9/2}$ (648, 653, 658, 664, 669, 674 nm) transitions [16–19,22–24]. As the Sm^{3+} doping concentration increases, the intensity of the emission peaks increases remarkably. However, a relatively high Sm^{3+} doping concentration (0.009 and 0.01) decreases the emission intensity due to the concentration quenching effect [25].

Fig. 5 shows the excitation spectra of the un-doped $Ca_2Sb_2O_7$ (λ_{em} = 605 nm) and $Ca_2Sb_2O_7$:$0.008Sm^{3+}$ (λ_{em} = 611 nm) samples. In order to provide a good explanation for the excitation process, the typical spectra were deconvoluted into separate Gaussian peaks. Doing so revealed that the excitation curve of $Ca_2Sb_2O_7$ could be resolved into two components: P_1 (269 nm) and P_2 (363 nm). Similarly, the excitation curve of $Ca_2Sb_2O_7$:$0.008Sm^{3+}$ consists of two single Gaussian peaks: P_3 (266 nm) and P_4 (302 nm). According to the above result, P_1 (269 nm) and P_3 (266 nm)